Magnetic phase transitions of $MnWO_4$ studied by the use of neutron diffraction

G. Lautenschläger
Fachbereich Materialwissenschaft, Fachgebiet Strukturforschung, Technische Hochschule Darmstadt, D-64287 Darmstadt, Germany and Institut Laue Langevin, F-38042 Grenoble, France

H. Weitzel
Fachbereich Materialwissenschaft, Fachgebiet Strukturforschung, Technische Hochschule Darmstadt, D-64287 Darmstadt, Germany

T. Vogt
Institut Laue Langevin, F-38042 Grenoble, France

R. Hock
Fachbereich Materialwissenschaft, Fachgebiet Strukturforschung, Technische Hochschule Darmstadt, D-64287 Darmstadt, Germany

A. Böhm
Institut für Festkörperphysik, Technische Hochschule Darmstadt, D-64287 Darmstadt, Germany

M. Bonnet
Centre d'Etudes Nucléaires de Grenoble, F-38041 Grenbole, France

H. Fuess
Fachbereich Materialwissenschaft, Fachgebiet Strukturforschung, Technische Hochschule Darmstadt, D-64287 Darmstadt, Germany
(Received 13 November 1992; revised manuscript received 28 April 1993)

Neutron-powder-diffraction data, collected with the D1B diffractometer, and single-crystal data, collected with the D10 four-circle diffractometer, both at the Institut Max von Laue–Paul Langevin, Grenoble, and single-crystal data, collected with the DN4 four-circle diffractometer at the Centre d'Etudes Nucléaires de Grenoble, show that $MnWO_4$ (space group $P2/c$) undergoes three magnetic phase transitions below 14 K. The transition temperatures are 13.5 K (paramagnet-AF3), 12.3 K (AF3-AF2), and 8.0 K (AF2-AF1). Phases AF3 and AF2 are incommensurate with the crystallographic lattice. The propagation vector is $\mathbf{k}=(-0.214,\frac{1}{2},0.457)$ in each case. In AF3 the magnetic moments order in the ac plane, whereas in AF2 an additional component in the [010] direction exists. The corresponding magnetic structures were found to be a sine wave in the case of AF3 and an elliptical spiral in the case of AF2. Other possibilities, like a simple spiral, a sine wave, and commensurate collinear spin arrangements, are also discussed for AF2. The magnetic structure in AF1 was refined based on a previously reported model. It is commensurate with a propagation vector $\mathbf{k}=(\pm\frac{1}{4},\frac{1}{2},\frac{1}{2})$. The magnetic moments are again collinear in the ac plane as in AF3, forming an angle of 37° with the a axis.

I. INTRODUCTION

$MnWO_4$ crystallizes in the wolframite structure and is isomorphous to other transition-metal tungstates as $FeWO_4$, $CoWO_4$, and $NiWO_4$. The structure is characterized by alternating layers of transition-metal and tungsten atoms parallel to the (100) plane. All cations are surrounded by distorted octahedra of hexagonal-close-packed oxygen ions which are aligned in zigzag chains along the c axis, as shown in Fig. 1. The symmetry of this structure is described within the monoclinic space group $P2/c$. The crystal structure parameters of these compounds were determined.[1]

The antiferromagnetic structures of $MnWO_4$,[2,3] $FeWO_4$,[4,5] $CoWO_4$,[5–7] $NiWO_4$,[5–7] and $(Mn,Fe)WO_4$ (Refs. 8 and 9) were already studied. The tungstates MWO_4 (M=Fe, Co, Ni) have a doubled magnetic unit cell $(2a,b,c)$, whereas the magnetic unit cell of $MnWO_4$ at 4.2 K is 16 times that of the crystallographic structure with magnetic lattice constants $4a$, $2b$, $2c$.

Specific-heat measurements on an $MnWO_4$ powder sample, pressed to a pellet, revealed three successive phase transitions.[10] The lowest at 6.8 K was attributed to the transition into the commensurate $(4a,2b,2c)$ phase, called here AF1. The other two transitions at 12.6 and 13.4 K, respectively, were also considered as magnetic transitions. In this context it should be mentioned that in earlier susceptibility measurements, only one transition could be resolved.[8]

The existence of these additional magnetically ordered phases, found in the specific heat, together with the four-fold magnetic periodicity in direction of the a axis, awoke our interest. It seems that these results can be understood in terms of the ANNNI model (axial next-nearest-neighbor Ising model).[11–13] Magnetic phase diagrams calculated within the ANNNI model show the following

features. (i) A large stability region for magnetic structures with fourfold periodicity along one of the crystallographic axes, i.e., a periodicity that can be described by a propagation vector of type $\mathbf{k}=\mathbf{G}/4$, $\mathbf{G}$ being a vector of the crystallographic reciprocal lattice. (ii) On varying the temperature as well as by applying an external magnetic field there are successive first-order transitions into different commensurate phases. (iii) All these phases converge towards a multicritical point.

Even if our suspicion that $MnWO_4$ could be a model system for the ANNNI model is speculative it will be interesting to characterize the low-temperature magnetic structures of $MnWO_4$, i.e., to investigate more closely the transitions found by the specific-heat measurements. Therefore we carried out a neutron-diffraction study in the temperature range 1.2–14 K and present the results in this paper.

Section II provides a characteristic of the samples, together with results from specific-heat and susceptibility measurements. In Sec. III the neutron-diffraction experiments are described. In Sec. IV a group-theoretical analysis of the problem is given. On the base of this analysis possible magnetic structures for all three phases are discussed in Sec. V. The results are finally summarized in Sec. VI.

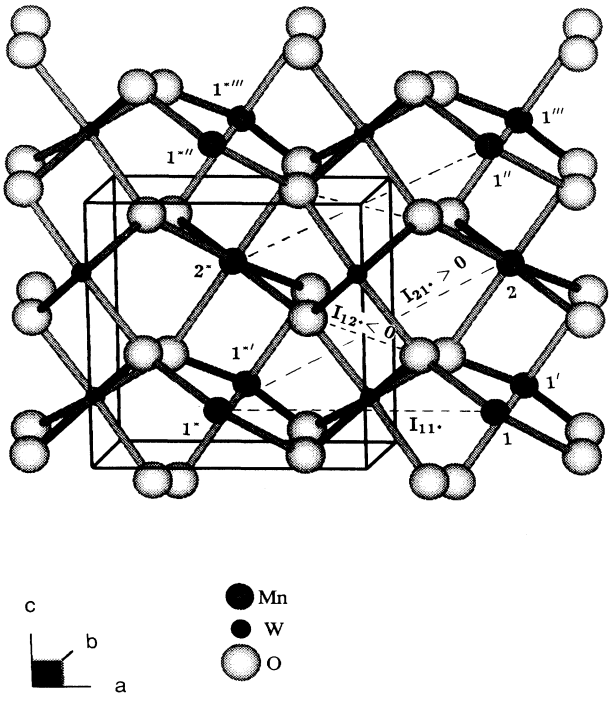

FIG. 1. Structure of $MnWO_4$; Mn and W atoms are surrounded by oxygen octahedra and are situated in layers parallel to the (100) plane; the numbers 1, 2 are attributed to the Mn^{2+} ions of the crystallographic unit cell, those of neighboring cells in *a*, *b*, and *c* direction are denoted by adding or removing the symbols *,','' in agreement with a previous publication (Ref. 5). The exchange interaction $I_{12}*$ is a superexchange via the common edge of two *W* octahedra; the competition $I_{12}*<0$, $I_{21}*>0$ leads to a frustration of $I_{11}*$.

II. SAMPLE CHARACTERIZATION

The $MnWO_4$ powder sample was prepared by solid-state reaction from stoichiometric mixtures of powders of MnO and WO_3. For the single-crystal experiments a natural $MnWO_4$ single crystal from Peru with a volume of 8 mm^3 was used. The iron content of this single-crystal sample was studied by x-ray Guinier powder diffraction from a powdered part of it and was found to be negligible.[8] In order to verify the previous results for the specific heat,[10] the specific heat of this single crystal was measured; it is given in Fig. 2. The twin peak, indicative for the two upper transitions, appears at 12.3 and 13.5 K, respectively, in good agreement with former results.[10] The transition peak from the intermediate phase AF2 to the low-temperature phase AF1 is broadened like a cusp and has its maximum at 8.0 K, whereas 6.8 K was reported for this transition.[10] The reason for these results seems to be due to the order of the transitions. From the shape of the peaks we conclude that the upper transitions are of second order, whereas the transition to the low-temperature phase AF1 is of first order. Furthermore, different transition temperatures for the same phase transition, here the transition AF2 to AF1, also suggest a first-order transition. In our case the different transition temperatures for this transition were obtained with a powder sample and a single crystal, respectively, so they could be due to grain-size effects.

In addition, the transition to the lowest phase AF1 and only to this phase can be influenced. We found this accidentally when we used another powder sample which was contaminated by small impurities of Mn_3O_4, which resulted from a different preparation method. For this sample especially, which was not investigated further by us, even at $T=1.7$ K there was still a contribution of the intermediate magnetic phase AF2 to the diffraction pattern, which was 15 times larger than in case of the above-mentioned first powder sample.

Figure 3 shows a susceptibility curve together with its derivative, which was obtained from the powder sample, on which we report in this paper. If one accepts the discontinuities in the derivative as transition tempera-

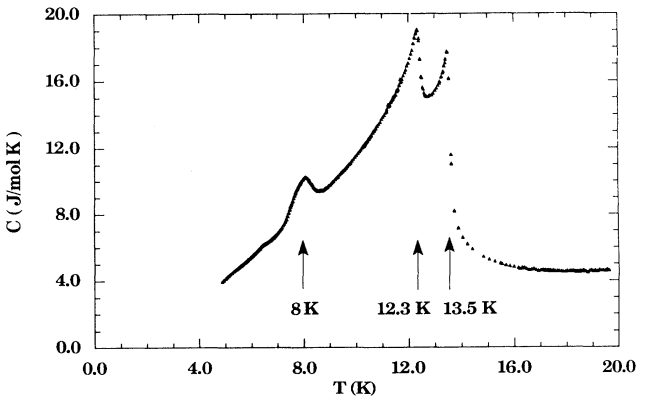

FIG. 2. Specific heat of the $MnWO_4$ single crystal plotted as function of temperature.

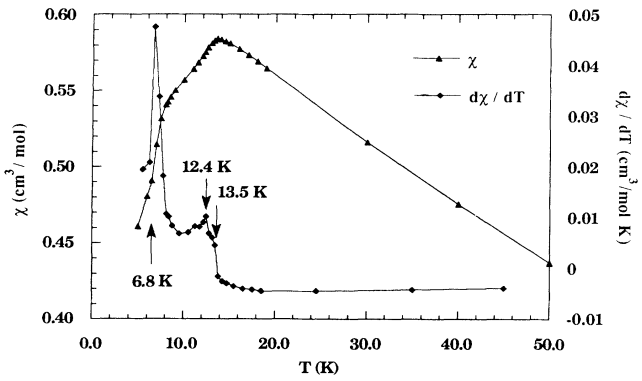

FIG. 3. Susceptibility of the $MnWO_4$ powder sample and its derivative plotted as a function of temperature.

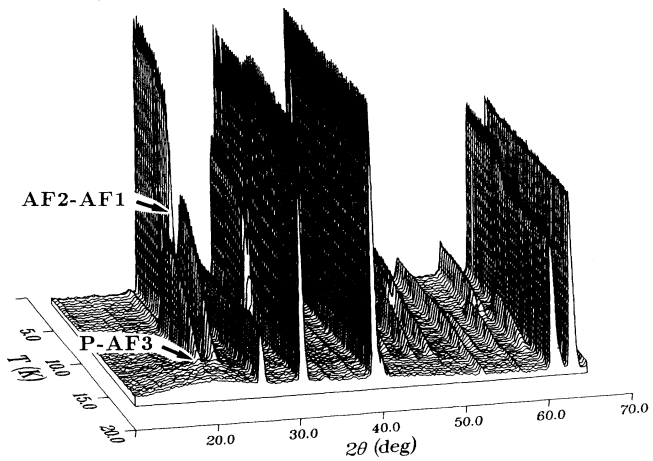

FIG. 4. Diffraction patterns measured at D1B, plotted as function of temperature. The transitions from the paramagnetic (P) phase to phase AF3, and from AF2 to AF1 are marked. The transition from AF3 to AF2 can hardly be recognized in the three-dimensional representation, see Fig. 8.

tures, then these temperatures are in good agreement with the specific-heat data[10] for all three transitions. In Table I all transition temperatures, which were obtained by the different methods from the different samples, are summarized.

III. NEUTRON-DIFFRACTION EXPERIMENTS

We collected neutron-diffraction patterns of $MnWO_4$ powder using the D1B diffractometer at the ILL (Ref. 14) in the temperature range between 1.2 and 14 K within 5 min per pattern in steps of 0.3 K over the whole temperature range. The angular range in 2θ was $10° \leq 2\theta \leq 80°$ in steps of 0.2°. Figure 4 displays the patterns. In order to separate magnetic reflections well from the nuclear scattering, we profited of the wavelength 2.529 Å used at D1B. A further powder pattern was measured at the high-resolution ILL diffractometer D1A (Ref. 14) at 1.5 K, using a wavelength of 1.909 Å. The recorded angular range in 2θ was $10° \leq 2\theta \leq 150°$, scanned in steps of 0.05°. The $MnWO_4$ single crystal was studied on the four-circle diffractometers D10 (Ref. 14) at the ILL and DN4 in the reactor SILOË of the CENG, the wavelength being 2.360 and 1.183 Å, respectively. At D10 we centered 96 magnetic satellites of the phase AF2 at 9.2 K and measured their intensities together with 21 nuclear reflections. In phase AF1, at 1.7 K, we measured 68 magnetic reflections together with the same nuclear reflections. Whereas at D10 no data set was collected of phase AF3, at DN4 nuclear and magnetic data sets of all three magnetic phases were collected at 5.2, 9.5, and 13.3 K. The number of measured nuclear reflections was 5 times bigger than in the case of the D10 experiment, in order to obtain a more accurate absolute value of the magnetic moment in each magnetic structure.

The data analysis of the powder patterns was performed using Rietveld profile refinement. The programs in use were FULLPROF (Ref. 15) for the 1.5 K pattern measured at D1A and MINREF (Ref. 16) for all other powder patterns. The calculated line shapes were pseudo-Voigt in the case of the D1A pattern and purely Gaussian for the D1B patterns. The background was determined by a linear interpolation between points in regions of the patterns without Bragg reflections.

The integrated intensities of the D10 experiment were also refined with the MINREF program. The structure factor for the commensurate phase AF1 was added to the subroutine which carries out the structure factor calculations. The magnetic lattice constants could be defined by use of the "special conditions" facility provided by MINREF. The residuals R_p and R_{wp} are defined as follows:

$$R_p = 100 \frac{\sum_{i=1}^{n} |y^i_{\text{obs}} - y^i_{\text{calc}}|}{\sum_{i=1}^{n} y^i_{\text{obs}}} ,$$

$$R_{wp} = 100 \left[\frac{\sum_{i=1}^{n} \frac{1}{\sigma_i^2} (y^i_{\text{obs}} - y^i_{\text{calc}})^2}{\sum_{i=1}^{n} \frac{1}{\sigma_i^2} (y^i_{\text{obs}})^2} \right]^{1/2} .$$

In case of the single-crystal data, the profile intensities without background y_i have to be replaced by integrated intensities.

TABLE I. Transition temperatures for the three magnetic phase transitions paramagnet (P)-AF3, AF3-AF2, and AF2-AF1, which were obtained by different methods from different sample types.

Technique	T(P-AF3) (K)	T (AF3-AF2) (K)	T (AF2-AF1) (K)	Sample type
$C(T)$	13.5	12.3	8.0	single crystal
$d\chi/dT$	13.5	12.4	6.8	powder
$C(T)$, Ref. 10	13.4	12.6	6.8	powder

IV. GROUP-THEORETICAL CONSIDERATIONS

Magnetic structures, which are compatible with the symmetry of the crystal structure, can be derived by Bertaut's group-theoretical method.[17] According to this method the coupling of the Fourier components of the magnetic moments is given by the basis vectors of one irreducible representation of the group $G_{\mathbf{k}}$, which is defined by the symmetry operations, under which the propagation vector $\mathbf{k}$ is invariant or only changed by a translation of the reciprocal lattice.

The space group of $MnWO_4$ is $G=P2/c$ with the general positions

$$(x,y,z),\quad (x,\bar{y},z+\tfrac{1}{2}),\quad (\bar{x},\bar{y},\bar{z}),\quad (\bar{x},y,\bar{z}+\tfrac{1}{2})\ .$$

The propagation vectors of the commensurate phase AF1 as well as of the incommensurate phases AF2 and AF3 are of the form $\mathbf{k}=(k_x,\frac{1}{2},k_z)$ as will be shown in Sec. V. Therefore the group of the propagation vector in both cases is

$$G_{\mathbf{k}}=Pc=\{(x,y,z),(x,\bar{y},z+\tfrac{1}{2})\}\ .$$

The positions of the two magnetic Mn^{2+} ions in the crystallographic unit cell are related by a glide reflection:

$$\mathbf{r}_1=\begin{bmatrix}0.5\\ y\\ 0.25\end{bmatrix},\quad \mathbf{r}_2=\begin{bmatrix}0.5\\ 1-y\\ 0.75\end{bmatrix}.$$

The transformation properties of the magnetic moments $\mathbf{m}_1$ and $\mathbf{m}_2$ under the elements of $G_{\mathbf{k}}$ define a representation

$$\Gamma=\Gamma_{\text{perm}}\times\Gamma_V$$

of 6×6 matrices, where Γ_V is the axial vector representation which describes the transformation of an axial vector under the symmetry elements of $G_{\mathbf{k}}$. By applying known relations,[17–20] the elements of Γ can be derived to be

$$\Gamma_{\text{perm}}[(x,y,z)]=\begin{bmatrix}1&0\\0&1\end{bmatrix},$$

$$\Gamma_{\text{perm}}[(x,\bar{y},z+\tfrac{1}{2})]=\begin{bmatrix}0&-a^2\\-1&0\end{bmatrix},$$

$$\Gamma_V[(x,y,z)]=\begin{bmatrix}1&0&0\\0&1&0\\0&0&1\end{bmatrix},$$

$$\Gamma_V[(x,\bar{y},z)]=\begin{bmatrix}-1&0&0\\0&1&0\\0&0&-1\end{bmatrix},$$

$$\Gamma[(x,y,z)]=\begin{bmatrix}1&0&0&0&0&0\\0&1&0&0&0&0\\0&0&1&0&0&0\\0&0&0&1&0&0\\0&0&0&0&1&0\\0&0&0&0&0&1\end{bmatrix},$$

$$\Gamma[(x,\bar{y},z+\tfrac{1}{2})]=\begin{bmatrix}0&0&0&a^2&0&0\\0&0&0&0&-a^2&0\\0&0&0&0&0&a^2\\1&0&0&0&0&0\\0&-1&0&0&0&0\\0&0&1&0&0&0\end{bmatrix},$$

with $a=e^{-i\pi k_z}$. For $G_{\mathbf{k}}$ there exist two one-dimensional irreducible representations Γ^{k1} and Γ^{k2}, given by

	(x,y,z)	$(x,\bar{y},z+\frac{1}{2})$
Γ^{k1}	1	a
Γ^{k2}	1	$-a$

Each irreducible representation enters three times into the representation Γ, i.e.,

$$\Gamma=3\Gamma^{k1}+3\Gamma^{k2}\ .$$

It follows that there are three basis vectors for each irreducible representation, the linear combination of which describe possible magnetic structures. They are given in Table II. According to these basis vectors the components of the magnetic moments have to be described by cosine functions

$$m_{j\alpha}(\mathbf{r})=m_{j\alpha}^{(0)}\cos(2\pi\mathbf{k}\cdot\mathbf{R}_l+\phi_{j\alpha}),\quad \alpha=x,y,z\ ,$$

$\mathbf{R}_l=l_1\mathbf{a}+l_2\mathbf{b}+l_3\mathbf{c}$, $(l_i=0,\pm1,\pm2,\ldots)$ being a translation vector of the crystallographic basis lattice. The phase relation between the two magnetic ions $j=1,2$ is

$$\phi_{2\alpha}=\phi_{1\alpha}+\pi k_z\ ,$$

and the amplitudes $m_{j\alpha}^{(0)}$ must be coupled as

$$m_{2x,z}^{(0)}=\pm m_{1x,z}^{(0)},\quad m_{2y}^{(0)}=\mp m_{1y}^{(0)}\ ,$$

corresponding to the two irreducible representations Γ^{k1} (upper sign) and Γ^{k2} (lower sign).

Depending on the choice of the amplitudes and phases these relations define sinusoidal structures as well as simple or elliptical spiral structures. A sine wave results for

$$\phi_{1x}=\phi_{1y}=\phi_{1z}\ ,$$

whereas a simple spiral can be defined by

$$m_{1x}^{(0)}=m_{1y}^{(0)}=m_{1z}^{(0)},\quad \phi_{1x}=\phi_{1z},\quad \phi_{1y}=\phi_{1x}+\pi/2\ .$$

TABLE II. Basis vectors of the group $G_{\mathbf{k}}$, corresponding to the irreducible representations Γ^{k1} and Γ^{k2}.

Representation	Γ^{k1}			Γ^{k2}		
Basis vector	1	2	3	1	2	3
Atom 1	1	0	0	1	0	0
	0	1	0	0	1	0
	0	0	1	0	0	1
Atom 2	a^*	0	0	$-a^*$	0	0
	0	$-a^*$	0	0	a^*	0
	0	0	a^*	0	0	$-a^*$

Collinear spin arrangements cannot be described within one irreducible representation if a y component of the magnetic moment exists. Nevertheless one has to keep in mind that a mixing of two irreducible representations can occur, because of the invariance of the exchange Hamiltonian under arbitrary rotations of the whole spin arrangement about any axis, causing an additional degeneracy. In this case the irreducible representations Γ_S^{kv} of the full symmetry group $G_k \times O_S \times I_S$ of the exchange Hamiltonian have to be considered, with O_S and I_S denoting the group of all rotations and the inversion group in spin space. By applying known relations[20] the representations Γ_S^{kv} can be decomposed into the irreducible representations of the group G_k,

$$\Gamma_S^{k1}=\Gamma^{k1}+2\Gamma^{k2}, \quad \Gamma_S^{k2}=2\Gamma^{k1}+\Gamma^{k2} .$$

As Γ^{k1} and Γ^{k2} enter into the decomposition, magnetic structures which are described by a combination of both irreducible representations are also possible.

V. RESULTS AND DISCUSSION

A. Commensurate phase AF1

The propagation vector in the phase AF1 was found to be $\mathbf{k}=(\pm\frac{1}{4},\frac{1}{2},\frac{1}{2})$ in accordance to the old results.[2,3] According to Sec. IV, the couplings of the Fourier components of the magnetic moments within the two irreducible representations are

$$\psi_{k1}=\begin{pmatrix} m_{1x}+im_{2x} \\ m_{1y}-im_{2y} \\ m_{1z}+im_{2z} \end{pmatrix}, \quad \psi_{k2}=\begin{pmatrix} m_{1x}-im_{2x} \\ m_{1y}+im_{2y} \\ m_{1z}-im_{2z} \end{pmatrix} .$$

Formally, these are sinusoidal or spiral structures with a phase shift of 90° between the Fourier component of the two magnetic ions. Nonmodulated structures can be derived as special cases of a sinusoidal structure, if the components of the propagation vectors adopt special values. This is visualized in Fig. 5. If one component of the propagation vector is $\frac{1}{4}$, the phase of the cosine function has to be an odd multiple of $\pi/4$ in order to get a nonmodulated structure. The value of the amplitude is then $\sqrt{2}$ times the real magnetic moment of the magnetic ions. In this way two nonmodulated structure models can be derived corresponding to the two irreducible representations. For $\mathbf{k}=(-\frac{1}{4},\frac{1}{2},\frac{1}{2})$ the signs of the x and z components of the magnetic moments in the magnetic unit cell **4a**, **2b**, **2c** in both cases are given in Fig. 6. For the y component the two schemes, shown in Fig. 6, have to be interchanged, i.e., a collinear spin arrangement is impossible within one irreducible representation if an additional y component exists. The same structure models were derived elsewhere by calculating the two-dimensional representations of the space group $P2/c$.[21]

According to former results,[2,3] the model corresponding to Γ^{k2} describes the magnetic structure in the phase AF1. A y component does not exist. In order to avoid confusion, it should be mentioned that in the previous papers[2,3] the setting up of the axes is **a**, $-$**b**, $-$**c** with respect

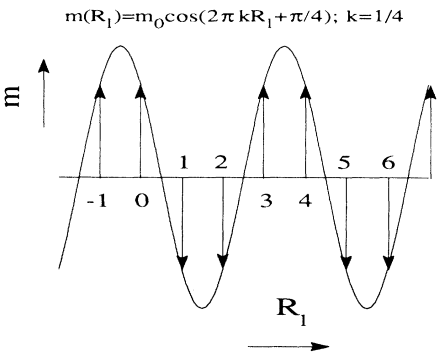

FIG. 5. Commensurate spin sequence for $k=\frac{1}{4}$ as a special case of a sinusoidal structure.

to our convention. This is the reason why there the other scheme, corresponding to Γ^{k1} in our convention, describes the magnetic structure. We tested these two models without and with a y component of the magnetic moment, as well as possible spiral structures. Finally agreement with previous results was obtained.[2,3] Powder and single-crystal data were fitted best by the model corresponding to Γ^{k2}, the magnetic moments having no y component. The results of the magnetic part of the refinements are tabulated in Table III. The spin direction is given in columns 5 and 6 of Table III in terms of the angles φ and ϑ. φ is the angle between the projection of the magnetic moments onto the ac plane and the a axis. ϑ is the angle between the magnetic moments and the b axis. In case of phase AF1 the magnetic moments order in the ac plane, therefore ϑ is 90°. Considering the variation of the value of the magnetic moment with temperature it can be seen that already at $T=5.2$ K the magnetic moments are almost saturated. The rather big value of the magnetic moment in case of the D10 experiment is due to the little number of nuclear reflections for the calibration of the intensities of the magnetic reflections.

The crystal structure parameters of the unit cell were only varied as least-squares parameters in case of the D1A powder pattern and kept fixed in all other cases. The starting values of the parameters for the refinement of the crystal structure were taken from a previous study.[1] No essential deviations from these data were found. The result of the crystal structure refinement of the D1A data is listed in Table IV. Figure 7 shows the corresponding observed and calculated intensities of the D1A powder pattern, as well as a difference plot. The

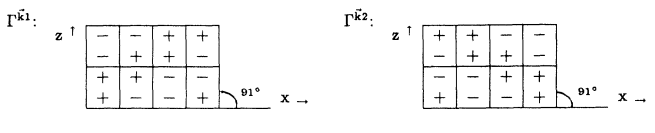

FIG. 6. Distribution of the signs of the x and z components of the magnetic moments, according to the irreducible representations Γ^{k1} and Γ^{k2} for $\mathbf{k}=(-\frac{1}{4},\frac{1}{2},\frac{1}{2})$; for the y component the two schemes have to be interchanged. One box represents a chemical unit cell.

TABLE III. Magnetic structural parameters of all three magnetically ordered phases. In the case of phase AF2 the cases (a), (b), and (c) correspond to refinements, assuming (a) a sinusoidal structure model with magnetic moments which have a y component, (b) a simple spiral, and (c) an elliptical spiral.

Technique	λ(Å)	T(K)	$\|\mathbf{m}\|(\mu_B)$	φ (°)	ϑ (°)	p	R_p	R_{wp}
			Low-temperature phase AF1					
powder (D1A)	1.909	1.5	4.5(1)	39.0	90.0		8.9	10.5
powder (D1B)	2.529	1.2	4.6(1)	39.3	90.0		7.1	8.1
single crystal (D10)	2.360	1.7	5.6(5)	36.6	90.0		8.6	10.2
single crystal (DN4)	1.183	5.2	4.5(1)	37.5	90.0		3.8	5.2
single crystal (Refs. 2 and 3)	1.08	4.2	4.4 (Ref. 9)	45(10)	90.0			
powder (Ref. 22)	1.069	4.2	4.8	54(7)	90.0		16	
			Intermediate phase AF2					
			(a)					
powder (D1B)	2.529	9.4	5.4(1)	32.5	49.6		7.9	8.5
single crystal (D10)	2.360	9.2	5.9(5)	35.8	52.1		4.2	6.0
single crystal (DN4)	1.183	9.5	5.3(1)	34.9	50.9		3.4	4.2
			(b)					
powder (D1B)	2.529	9.4	3.8(1)	31.9		1.0	7.9	8.7
single crystal (D10)	2.360	9.2	4.5(5)	32.8		1.0	8.2	10.8
single crystal (DN4)	1.183	9.5	3.8(1)	33.6		1.0	6.6	8.9
			(c)					
powder (D1B)	2.529	9.4	3.9(1)	35.9		0.99	7.9	8.6
single crystal (D10)	2.360	9.2	4.8(5)	34.6		0.78	4.6	6.8
single crystal (DN4)	1.183	9.5	4.1(1)	33.9		0.82	3.5	4.3
			High-temperature phase AF3					
powder (D1B)	2.529	12.7	2.3(1)	35.0	90.0		7.5	7.6
single crystal (DN4)	1.183	13.3	2.1(1)	34.8	90.0		5.4	7.4

positions of the nuclear reflections are marked by the upper line of bars, the positions of the magnetic ones by the lower line.

Characteristic for the magnetic structure of AF1 are the double stripes of + and − signs, denoting spin up and spin down for the Mn^{2+} ions (see Fig. 6). It was shown[5] that this structure can be understood, assuming exchange interactions $I_{12*}(=I_{21*,,})<0$, $I_{21*}(=I_{1''2*})>0$, and $I_{21*'}<0$ as the dominating ones, where 1,2 number the Mn^{2+} ions of the crystallographic unit cell and the symbols *,′, and ″ denote those of neighboring cells in a, b, and c directions in agreement with a previous publication.[5] In Fig. 1 the path of the exchange interaction I_{12*} is shown, which is a 180° Me-O-O-Me superexchange via the common edge of two W octahedra. The positive exchange I_{21*} is also included in Fig. 1. From these two competing exchange interactions a frustration of the exchange I_{11*} results.

TABLE IV. Crystal structure parameters refined from the D1A powder pattern at 1.5 K.

	Lattice constants			
	a	b	c	β
	4.8226(3)	5.7533(6)	4.9923(5)	91.075(7)
	Positional parameters			
	x	y	z	B
Mn	0.50	0.6853(4)	0.25	0.14(4)
W	0.00	0.1795(4)	0.25	0.06(4)
O_I	0.2108(3)	0.1024(2)	0.9419(2)	0.21(3)
O_{II}	0.2516(2)	0.3752(2)	0.3931(2)	0.25(2)

Reliability factors $R_p=8.9$, $R_{wp}=10.5$

B. Incommensurate phases AF2 and AF3

1. *Sinusoidal structures*

Figure 8 shows the evolution of the D1B powder patterns with temperature. At about 13.6 K, in the 2θ range

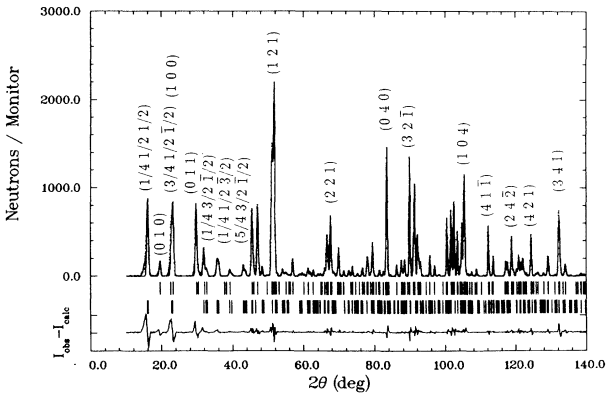

FIG. 7. Observed and calculated powder pattern of phase AF1 at $T=1.5$ K, $\lambda=1.909$ Å.

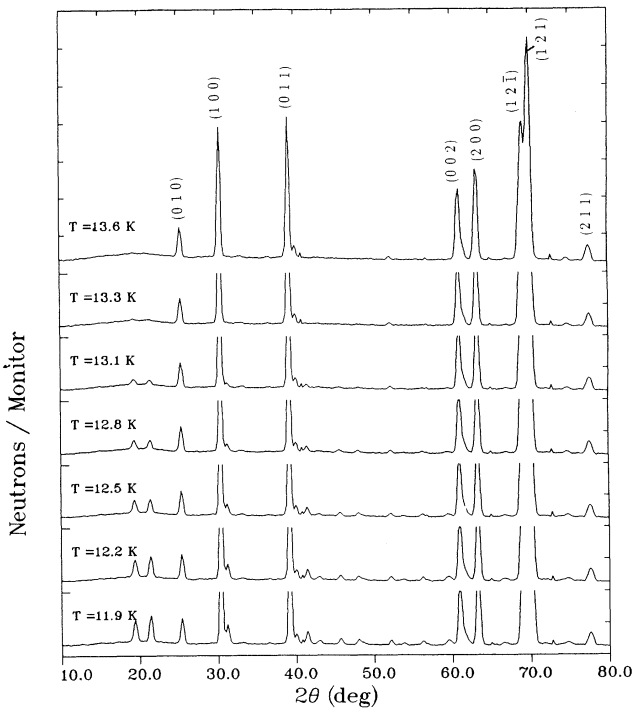

FIG. 8. Temperature evolution of the D1B powder patterns between 13.6 and 11.9 K.

$10° \leq 2\theta \leq 24°$ the background is enhanced, due to diffuse magnetic scattering. At 13.1 K the two strongest magnetic satellites appear out of this diffuse magnetic background. Other magnetic satellites follow in positions up to 70° in 2θ. The satellite intensities grow with decreasing temperature and reach a maximum at 8.5 K (not shown in Fig. 8). At first sight only one magnetic phase seems to exist, and a shift of the satellite positions, indicative of a change of the magnetic periodicity, cannot be observed. Nevertheless it can be recognized that down to 12.5 K the first two magnetic satellites have equal intensity, but that on further cooling the one at $2\theta = 21.4°$ increases more rapidly. This shows that, despite no change of the magnetic periodicity, the spin orientations with respect to the corresponding reflection planes change at about 12.5 K.

We recognized soon that the magnetic periodicity in reciprocal space could not be expressed by simple rational fractions of the periodicity of the crystal structure. The application of a method for indexing the satellites in powder patterns was finally successful.[23] It was found that the positions of the magnetic satellites can be described by vectors $\mathbf{K}_i$ in reciprocal space, which have the form $\mathbf{K}_i = \mathbf{G}_i \pm \mathbf{k}$, where $\mathbf{G}_i$ is a vector of the nuclear reciprocal lattice and $\mathbf{k}$ is the propagation vector. The propagation vector found by this method was $\mathbf{k} = (-0.205, 0.495, 0.457)$. The single-crystal experiment, carried out at D10, confirmed this result within the experimental error. The wave vector, as it turns out from the Rietveld refinements of the magnetic structures by means of the powder patterns is $\mathbf{k} = (-0.214, \frac{1}{2}, 0.457)$. Without affecting the goodness of fit the y component of the wave vector could be fixed to be $\frac{1}{2}$.

According to Sec. IV for such a wave vector only sinusoidal or spiral structures are possible within the predictions of group theory. Therefore we began the search for suitable structural models by applying the models, proposed by group theory, on the D1B powder patterns. The patterns, recorded in the upper phase AF3, can be fitted well, assuming sinusoidally modulated magnetic moments which are aligned in the ac plane. The angle with the a axis is almost that of the commensurate phase AF1. The coupling of the Fourier components of the magnetic moments in the chemical unit cell is given by the basis vectors, corresponding to the irreducible representation Γ^{k2}, i.e.,

$$\phi_{2\alpha} = \phi_{1\alpha} + \pi k_z \ ,$$

$$m^{(0)}_{2x,z} = -m^{(0)}_{1x,z}, \quad m^{(0)}_{2y} = m^{(0)}_{1y} = 0 \ .$$

Figure 9 shows the observed and calculated pattern for this model. The refined spin direction and the magnetic moment are listed in Table III.

The magnetic structure of the intermediate phase AF2 was more difficult to determine. Among the models left within one irreducible representation of the wave-vector group, the best result was obtained by adopting the same model as for AF3. Figure 10(a) shows the corresponding difference plot. In the lower 2θ region the intensities are not fitted very well, especially the reflection $(111)^-$, which is marked by an arrow, is only at about 10% of its measured intensity.

A more satisfying fit could only be reached by combining the two irreducible representations Γ^{k1} and Γ^{k2}. If the y components of the magnetic moment couple according to Γ^{k1} and the x and z components according to Γ^{k2}, all three components couple in the same way and a collinear structure with y component results. This is not possible within only one irreducible representation. As a second-order transition takes place involving only one single irreducible representation of the group G_k the cou-

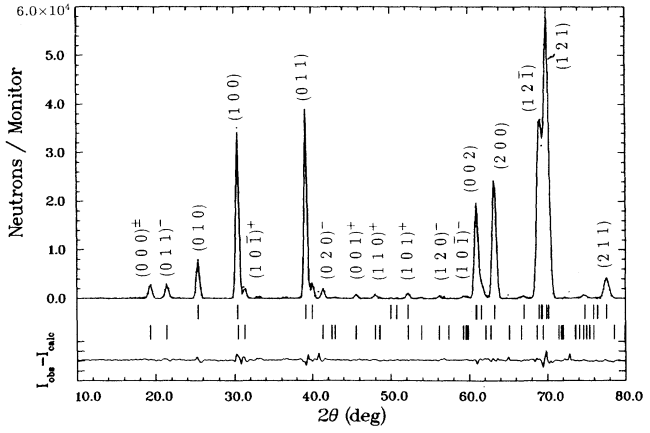

FIG. 9. Powder patterns of phase AF3, at $T = 12.7$ K; the magnetic part is calculated with a collinear sinusoidal structure, having no component in the [010] direction. The indices $(hkl)^{\pm}$ stand for $(hkl) \pm \mathbf{k}, \mathbf{k} = (-0.214, \frac{1}{2}, 0.457)$.

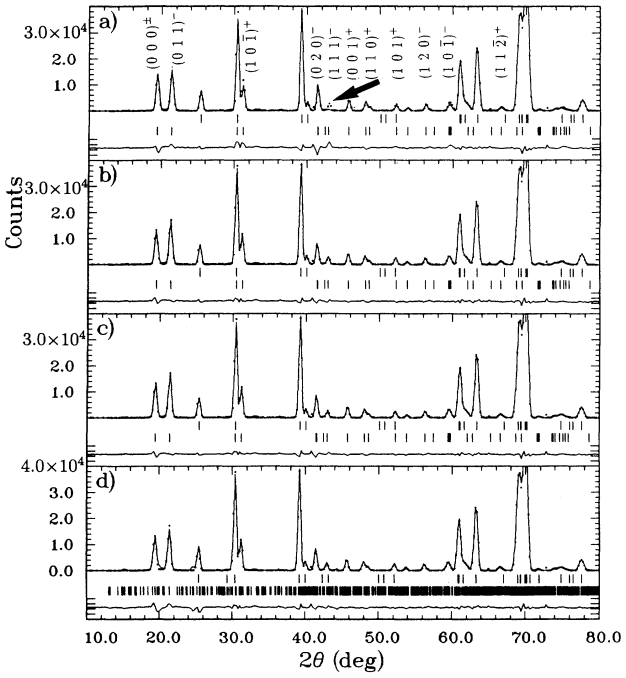

FIG. 10. Powder patterns of phase AF2 at $T=9.4$ K. The magnetic scattering intensity is calculated with models (a) sinusoidal structure without component in [010] direction; (b) same as (a) but with an additional component in [010] direction; (c) elliptical spiral structure; (d) collinear commensurate spin arrangement in the magnetic unit cell **14a,2b,35c**.

pling of the y components according to another irreducible representation than that of the x and z components requires that phase AF2 arises by two successive second-order phase transitions, the first from the paramagnetic state to phase AF3 via Γ^{k2} and the second from phase AF3 to phase AF2 via Γ^{k1}. This is exactly what we observed. The phase AF3 possesses ordered x and z components and an unordered y component. Such states are called "semiordered."[20] Similar arguments have been applied to explain the spiral cone structure of $MnSO_4$ at 4.2 K, which arises in even three successive phase transitions.[24,25] The fit we obtained, by assuming the collinear sinusoidal structure with magnetic moments pointing in a general direction, is shown in Fig. 10(b). The results of these refinements are listed in Table III, part (a).

The existence of the y component of the magnetic moments is additionally confirmed by the susceptibility versus temperature behavior of our single crystal in the [010] direction, which is shown in Fig. 11.

The problematic feature of the sinusoidal structure is that it does not preserve the monoclinic symmetry, in disagreement with our single-crystal data. Within the experimental error the integrated intensities, measured at the four-circle diffractometers D10 and DN4, fulfill the condition $I(hkl)=I(h\bar{k}l)$. This problem can be solved by assuming the existence of two spin domains which are related by the monoclinic mirror plane. The powder data are not affected by this, as only the sum $I(hkl)+I(h\bar{k}l)$ can be resolved in a powder pattern. Looking at the

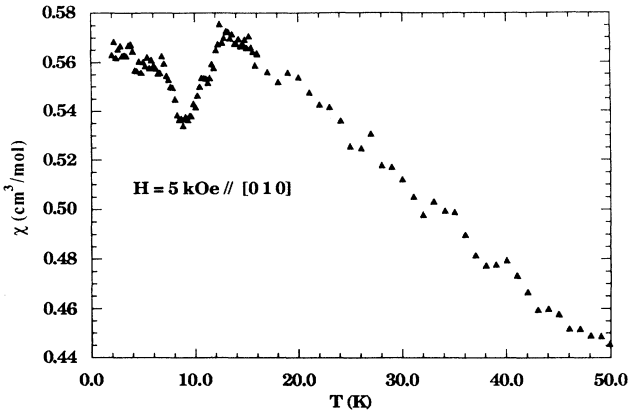

FIG. 11. DC susceptibility of the $MnWO_4$ single crystal measured in the [010] direction.

refined values for the magnetic moment, a new problem arises, although the obtained agreement between measured and calculated data is satisfactory. The magnetic moment in the phase AF2 turns out to be higher than in the low-temperature phase AF1 and even higher than the theoretical value of $5\mu_B$ for Mn^{2+}. One must bear in mind that the values given in Table III, part (a) are the amplitudes of a cosine function, whereas the real magnetic moment on site j in cell $\mathbf{R}_l$ is given by $\mathbf{m}_j=\mathbf{m}_0\cos(2\pi\mathbf{k}\cdot\mathbf{R}_l+\theta_j)$ and so in general is lower than the amplitude. Nevertheless, because of the incommensurate values of the wave vector's x and z component, there are sites where the cosine function is almost 1.

For this reason we looked for further structures, giving similar diffraction patterns as the described sine wave. Two further possibilities were considered: a spiral, with magnetic moments coupled in the same way as in case of the sine wave, and a commensurate collinear spin arrangement with a very large magnetic unit cell, which can be described approximately by the sine wave presented above.

2. *Spiral structures*

A simple spiral, expressed in general by

$$\mathbf{m}(\mathbf{R}_l)=m_0[\mathbf{u}\cos(2\pi\mathbf{k}\cdot\mathbf{R}_l+\phi)+\mathbf{v}\sin(2\pi\mathbf{k}\cdot\mathbf{R}_l+\phi)]\ ,$$

$$|\mathbf{u}|=|\mathbf{v}|=1,\quad \mathbf{u}\perp\mathbf{v}\ ,$$

has a structure factor, which is a factor $\sqrt{2}$ times that of the corresponding sine wave

$$\mathbf{m}(\mathbf{R}_1)=m_0[\mathbf{u}\cos(2\pi\mathbf{k}\cdot\mathbf{R}_1+\phi)]\ ,$$

if the wave vector is perpendicular to the spin direction, i.e., if the condition

$$\mathbf{k}\perp\mathbf{u}\perp\mathbf{v}$$

is fulfilled. In this case the diffraction patterns are identical. Only the refined magnetic moment appears to be lower by a factor $1/\sqrt{2}$ for the spiral. Although the wave vector is not perpendicular to the spin direction obtained from the sine wave, it is possible to find a spiral

structure with a similar diffraction pattern, if the vectors $\mathbf{u}_i$ and $\mathbf{v}_i$ $(i=1,2)$ which define the basal planes of the two spirals corresponding to the two magnetic moments of the chemical unit in $MnWO_4$ are chosen to be

$$\mathbf{u}_i=\begin{bmatrix} u_{ix} \\ 0 \\ u_{iz} \end{bmatrix}, \quad \mathbf{v}_i=\begin{bmatrix} 0 \\ 1 \\ 0 \end{bmatrix} .$$

The amplitude vectors and the phases have to be coupled as

$$\mathbf{u}_2=-\mathbf{u}_1, \quad \mathbf{v}_2=-\mathbf{v}_1, \quad \phi_2=\phi_1+\pi k_z .$$

Because of the special choice of the vectors $\mathbf{u}_i$ and $\mathbf{v}_i$ for this structure, $I(hkl)=I(h\bar{k}l)$ is fulfilled within one domain so that averaging over different spin domains is not necessary.

The results obtained with this structure are given in Table III, part (b). The angle φ is now the angle between the vectors $\mathbf{u}_i$ and the a axis. It can be seen that the value of the magnetic moment has dropped and that the agreement between observed and calculated data is reasonable. Nevertheless, especially for the single-crystal data the agreement was still better for the sinusoidal structure with two spin domains.

At the phase transition AF3-AF2 the ordering of the so-far paramagnetic y component of the magnetic moments begins. As the temperature evolution of this additional ordering is independent from the ordering of the component in the ac plane, there is no physical reason that these two components have the same magnitude as in a simple spiral. Therefore we allowed as a further degree of freedom the simple spiral to become elliptical. The elliptical spiral is described by the equation

$$\mathfrak{m}(\mathbf{R}_l)=m_0[\mathbf{u}\cos(2\pi\mathbf{k}\cdot\mathbf{R}_l+\phi)+\mathbf{v}p\sin(2\pi\mathbf{k}\cdot\mathbf{R}_l+\phi)] ,$$
$$|\mathbf{u}|=|\mathbf{v}|=1$$

with the parameter $p\neq 1$. With this structure finally the same agreement between calculated and observed data was obtained as with the sinusoidal structure, but giving a more reasonable value for the magnetic moment of Mn^{2+}. The results are given in Table III, part (c). Because of the independent temperature evolution of the y component of the magnetic moment, which is the minor axis of the ellipse, the parameter p is temperature dependent and increases with decreasing temperature. In Table III, part (c), comparing the p values obtained from the D10 and DN4 data at 9.2 and 9.5 K, this is only fulfilled within an experimental error of 0.05. This is mainly due to the fact that the absolute-temperature values obtained from the two thermometers in use for both experiments probably differ by some zero shift. In order to study the temperature dependence of p the intensity of a reflection, which is sensitive to the presence of a y component of the magnetic moment, e.g., the reflection $(111)^-$, has to be measured as a function of temperature. Preliminary results were obtained; a full account will be given elsewhere.

Figure 10(c) shows the difference plot, corresponding to the refinement of the elliptical spiral. It turns out that in the powder pattern circular and elliptical spirals are indistinguishable whereas the single-crystal data are fitted significantly better in the case of the elliptical spiral. The observed and calculated single-crystal data are listed in Table V.

TABLE V. Observed and calculated magnetic integrated intensities of the D10 experiment at 9.2 K.

hkl	I_{calc}	I_{obs}	hkl	I_{calc}	I_{obs}
$(0\bar{1}0)^+$	27.14	27.29	$(000)^+$	27.14	27.52
$(000)^-$	27.14	27.39	$(001)^-$	42.95	42.82
$(011)^-$	42.95	42.56	$(0\bar{1}\bar{1})^+$	42.95	42.12
$(1\bar{1}0)^+$	12.03	11.94	$(\bar{1}10)^-$	12.03	11.82
$(100)^+$	12.03	12.11	$(\bar{1}00)^-$	12.03	12.00
$(1\bar{1}\bar{1})^+$	55.44	54.28	$(\bar{1}11)^-$	55.44	50.05
$(10\bar{1})^+$	55.44	47.74	$(\bar{1}01)^-$	55.44	49.24
$(0\bar{2}0)^+$	49.54	51.40	$(0\bar{1}0)^-$	49.54	48.39
$(100)^-$	17.70	18.49	$(\bar{1}00)^+$	17.70	17.68
$(110)^-$	17.70	16.66	$(0\bar{1}1)^-$	1.44	1.52
$(0\bar{2}\bar{1})^+$	1.44	1.53	$(101)^-$	21.63	22.09
$(111)^-$	21.63	21.48	$(0\bar{1}1)^+$	42.03	38.50
$(01\bar{1})^-$	42.03	40.98	$(001)^+$	42.03	38.81
$(00\bar{1})^-$	42.03	37.84	$(1\bar{2}0)^+$	34.78	32.67
$(00\bar{2})^+$	14.08	13.56	$(002)^-$	14.08	13.60
$(012)^-$	14.08	13.59	$(0\bar{1}\bar{2})^+$	14.08	13.69
$(1\bar{2}\bar{1})^+$	1.49	1.20	$(1\bar{1}1)^+$	21.44	22.60
$(101)^+$	21.44	22.19	$(10\bar{2})^+$	17.13	16.56
$(\bar{1}02)^-$	17.13	16.19	$(1\bar{1}\bar{2})^+$	17.13	15.95
$(\bar{1}12)^-$	17.13	15.53	$(1\bar{1}0)^-$	37.42	37.76
$(1\bar{1}1)^-$	0.84	1.13	$(121)^-$	0.84	0.89
$(11\bar{1})^-$	34.53	34.03	$(10\bar{1})^-$	34.53	33.77
$(\bar{1}01)^+$	34.53	34.04	$(2\bar{1}0)^+$	7.02	6.78
$(\bar{2}10)^-$	7.02	7.33	$(200)^+$	7.02	6.93
$(\bar{2}00)^-$	7.02	7.46	$(0\bar{2}1)^+$	1.21	1.43
$(011)^+$	1.21	1.37	$(0\bar{1}\bar{1})^-$	1.21	1.44
$(2\bar{1}\bar{1})^+$	25.92	26.18	$(\bar{2}11)^-$	25.92	26.85
$(20\bar{1})^+$	25.92	23.79	$(\bar{2}01)^-$	25.92	26.36
$(0\bar{1}2)^-$	31.21	32.26	$(0\bar{2}\bar{2})^+$	31.21	32.54
$(022)^-$	31.21	31.62	$(102)^-$	6.21	6.31
$(112)^-$	6.21	6.62	$(1\bar{2}1)^+$	0.75	1.99
$(111)^+$	0.75	1.30	$(11\bar{2})^+$	35.38	35.86
$(1\bar{2}\bar{2})^+$	35.38	35.46	$(\bar{1}22)^-$	35.38	36.50
$(0\bar{3}0)^+$	1.31	1.77	$(0\bar{2}0)^-$	1.31	1.79
$(0\bar{2}1)^-$	23.18	25.44	$(0\bar{3}\bar{1})^+$	23.18	23.67
$(12\bar{1})^-$	1.02	1.34	$(1\bar{1}\bar{1})^-$	1.02	1.51
$(\bar{1}11)^+$	1.02	1.38	$(2\bar{2}0)^+$	18.14	19.35
$(\bar{2}20)^-$	18.14	20.41	$(210)^+$	18.14	20.33
$(2\bar{2}\bar{1})^+$	0.82	0.80	$(\bar{2}21)^-$	0.82	0.80
$(21\bar{1})^+$	0.82	0.82	$(1\bar{3}0)^+$	1.05	1.79
$(2\bar{2}\bar{1})^+$	7.32	7.59	$(\bar{1}\bar{1}0)^-$	7.32	7.82
$(2\bar{1}\bar{1})^-$	7.32	7.39	$(1\bar{3}\bar{1})^+$	22.27	22.35
$(1\bar{1}2)^-$	16.22	17.37	$(122)^-$	16.22	16.94
$(2\bar{2}0)^-$	10.87	10.78	$(2\bar{1}0)^-$	10.87	10.95
$(2\bar{1}1)^+$	9.15	9.51	$(201)^+$	9.15	9.58
$(2\bar{1}\bar{2})^+$	9.52	10.30	$(\bar{2}12)^-$	9.52	10.05
$(20\bar{2})^+$	9.52	9.76	$(\bar{2}02)^-$	9.52	9.69

$R_p=4.6$, $R_{wp}=6.8$

3. *Commensurate collinear structures*

Although in the case of a commensurate collinear structure with saturated magnetic moments the Fourier series has to contain higher harmonics which we could not detect so far, we calculated the diffraction patterns for such structures. First a suitable commensurate magnetic unit has to be determined, compatible with the propagation vector $\mathbf{k}=(-0.214,\frac{1}{2},0.457)$. By developing the x and z components of $\mathbf{k}$ in Eulerian continued fractions we found that they can be approximated by

$$k_x=-0.214\approx-\tfrac{3}{14}=-0.2143\ ,$$

$$k_z=0.457\approx\tfrac{5}{11}=0.4545\ \text{ or }\ k_z=0.457\approx\tfrac{16}{35}=0.4571\ .$$

A magnetic unit cell 14**a**, 2**b**, 11**c** or better 14**a**,2**b**,35**c** has to be assumed in order to obtain the translational symmetry given by the propagation vector. The latter cell contains 980 chemical unit cells with 1960 magnetic ions.

It is worth mentioning that the fraction $-\frac{3}{14}$, which was found for k_x, obeys the building law

$$\tfrac{3}{14}=\frac{i}{2(2i+1)}\quad\text{for } i=3\ .$$

This building law is derived within the framework of the ANNNI model.[12] In the ANNNI model the magnetic ions are situated in ferromagnetic planes with competitive ferromagnetic and antiferromagnetic interactions between planes. The propagation vector given by this building law describes the translational symmetry perpendicular to these planes.

In our case the Mn^{2+} ions are also located in planes. Although antiferromagnetic, these planes are parallel to the (100) plane and perpendicular to the periodicity given by $k_x=-\frac{3}{14}$. Another possibility is to consider k_x as well as k_z as fractions within the predictions of the ANNNI model, giving rise to an ANNNI-model-like behavior in two dimensions. The corresponding planes in direct space which are almost perpendicular to the projection $(-\frac{3}{14},0,\frac{16}{35})$ of $\mathbf{k}$ into the a^*c^* plane, are then the (-102) planes. The exact angle is 88.5°. In this sense the first-order phase transition AF1-AF2 could be described by the ANNNI model, although the change of the spin direction during this phase transition shows that $MnWO_4$ is not an Ising system.

In order to carry out calculations for commensurate models we had to find suitable mutual orientations of the magnetic moments in the large unit cells, given above. In order to be as close as possible to the sine wave structure, the commensurate structure was assumed to be a square wave, which was generated by the function

$$\mathbf{m}(\mathbf{R}_l)=m_0\{\mathbf{u}\,\mathrm{sgn}[\cos(2\pi\mathbf{k}\cdot\mathbf{R}_l+\phi)]\}$$

from the sine wave. The direction of the magnetic moments was taken from the refinement of the sine wave in Table III, part (a). Figure 12 shows a graphical representation of this procedure for the case $k_x=-\frac{3}{14}$, $k_z=\frac{5}{11}$, i.e., a magnetic unit cell 14**a**, 2**b**, 11**c**. Powder patterns are calculated with magnetic unit cells 14**a**,2**b**,11**c** and 14**a**, 2**b**, 35**c**; the latter is shown in Fig. 10(d). The results are given in Table VI, together with the results obtained from the single-crystal data. The magnetic moment we obtained is almost equal to the moment as refined from the elliptical spiral. It can be recognized that in spite of the large number of reflections which arise from such a unit cell, the powder pattern shown in Fig. 10(d) is quite similar to that of the sinusoidal structure [Fig. 10(b)] as most of the additional reflections appear to be quasiextinguished. Nevertheless some small additional peaks exist, which do not appear in the observed pattern. It cannot be excluded that they can be eliminated by subtle changes of the spin direction or by inverting some spins of the magnetic unit cell.

From the results given above, the elliptical spiral appears to be the most suitable model for the magnetic structure in the phase AF2, but nevertheless our considerations concerning an eventual commensurability of AF2 remain valid. They are underlined by the fact that no shift of the propagation vector with temperature could be observed. In terms of magnetic exchange the magnetic structure behavior of $MnWO_4$ seems to arise from the competitive exchange interactions between zigzag chains of Mn^{2+} within the layers, neighbored in [100] direction,

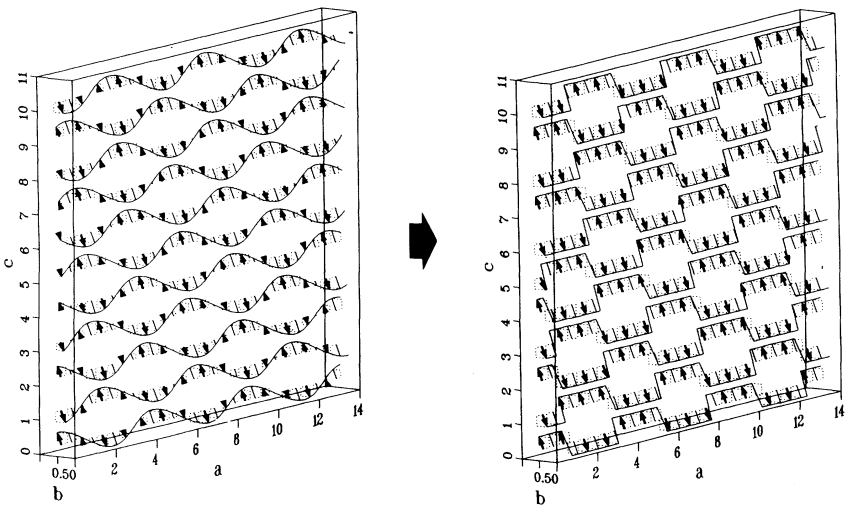

FIG. 12. Construction principle for commensurate magnetic structure models from an underlying sine wave. Only one magnetic moment per crystallographic unit cell is plotted. The numbers are the numbers of the chemical unit cells in the directions **a**, **b**, and **c**.

TABLE VI. Magnetic structural parameters of phase AF2 as obtained under the assumption of a commensurate collinear spin arrangement in magnetic unit cells **14a,2b,11c** and **14a, 2b,35c**, respectively.

	Powder (D1B)			Single crystal (D10)			Single crystal (DN4)		
Cell	$\|\mathbf{m}\|$ (μ_B)	R_p	R_{wp}	$\|\mathbf{m}\|$(μ_B)	R_p	R_{wp}	$\|\mathbf{m}\|$ (μ_B)	R_p	R_{wp}
14-2-11	4.1	10.3	12.6	4.7	6.4	8.1	4.2	4.6	6.0
14-2-35	4.1	9.1	11.2	4.7	6.3	8.1	4.2	4.6	6.0

as described,[5] in order to explain the commensurate phase AF1. The occurrence of three magnetic phases has its origins in a competition between isotropic exchange interactions and single-ion anisotropy. The single-ion anisotropy, which is due to the interaction of the magnetic moments with the crystal field, prefers an alignment of the magnetic moments in the so-called easy direction, i.e., the direction of the magnetic moments in phases AF3 and AF1. The incommensurate translation symmetry of phases AF3 and AF2 has its origin in competing isotropic exchange interactions, underlined by the occurrence of the two irreducible representations, which are degenerated in the higher symmetry of the exchange group. This degeneracy is destroyed by single-ion anisotropy. Therefore on cooling from the paramagnetic state, in phase AF3 the magnetic moments begin to order according to one irreducible representation. By virtue of the anisotropy they are aligned in the easy direction, but with the incommensurate translation symmetry, which is described by the wave vector $\mathbf{k}=(-0.214,\frac{1}{2},0.457)$. The component in the [010] direction is not ordered in phase AF3, so this phase can be called semiordered. For entropy reasons—the magnetic moments tend to saturate—the collinear sine wave structure of phase AF3 cannot be stable. Therefore in a further transition, the component in the [010] direction orders, leading to the observed elliptical spiral structure in phase AF2, where in principle the magnetic moments could saturate. The spiral however is not preferable for the anisotropy. Therefore with decreasing temperature, where the contribution of the anisotropic term in the Hamiltonian becomes more and more important, the transition to the commensurate phase AF1 occurs, where again the magnetic moments are aligned in the *ac* plane in the easy direction and in addition have the possibility to saturate.

In order to proceed further in answering the question "incommensurate elliptical spiral or long period commensurate collinear spin arrangement for the phase AF2," we intend to carry out a further experiment with a bigger crystal, in order to look for the higher harmonics. In case of the sinusoidal structure AF3, a spin-density measurement with polarized neutrons could be instructive. The predictions of the ANNNI model concerning the presence of several further magnetic phases in presence of a magnetic field are just being investigated by field-dependent single-crystal experiments.

VI. CONCLUSION

We have studied the three magnetic phases of $MnWO_4$ in the temperature range $T=1.2$ K to $T=14$ K by means of neutron diffraction and supplementary specific-heat and susceptibility measurements. It turned out that the two upper phases AF2 and AF3, which exist in the temperature ranges $T=8.0-12.3$ K and $T=12.3-13.5$ K, are antiferromagnetic. The translational symmetry appears to be the same in both phases. It can be described by a propagation vector $\mathbf{k}=(-0.214,\frac{1}{2},0.457)$. The main difference between the magnetic structures is the existence of a component of the magnetic moments in the [010] direction in phase AF2, which does not exist in AF3. The best agreement between observed and calculated neutron data was obtained by assuming a sinusoidal modulation of the magnetic moments in the phase AF3, and an elliptical spiral structure in AF2. The basal plane of the elliptical spiral contains the *b* axis and intercepts the *ac* plane in the direction of the magnetic moments of AF3.

Commensurate collinear models, which appear in predictions of the ANNNI model, are discussed for the phases AF1 and AF2. For AF2 the agreement between calculations and experiments for the commensurate models assumed is not as good as in the case of the elliptical spiral. Nevertheless further experiments, especially in presence of a magnetic field, will be of interest to investigate this point in more detail.

The commensurate phase AF1 was found to be identical with former results.[2,3] Its translational symmetry is described by a propagation vector $\mathbf{k}=(\pm\frac{1}{4},\frac{1}{2},\frac{1}{2})$. The magnetic moments are aligned collinear in the *ac* plane, forming an angle of 37° with the *a* axis.

ACKNOWLEDGMENTS

The authors are grateful to Dr. M. Reehuis, who performed the measurement of the powder susceptibility at the Anorganisch Chemisches Institut of the University Münster and to R. Chagnon for his technical support during the D10 experiment. Further, we thank Dr. J. K. Cockcroft for the permission to use his structure plot program JACKAL. This work has been supported by the German Federal Minister for Research and Technology (BMFT) under Contract Nos. 03WL2DAR8 and 03FU3DAR.

[1]H. Weitzel, Z. Kristallogr. **144**, 238 (1976).
[2]H. Dachs, H. Weitzel, and E. Stoll, Solid State Commun. **4**, 473 (1966).
[3]H. Dachs, E. Stoll, and H. Weitzel, Z. Kristallogr. **125**, 121 (1967).
[4]D. Ülkü, Z. Kristallogr. **124**, 192 (1967).
[5]H. Weitzel and H. Langhof, J. Magn. Magn. Mater. **4**, 265 (1977).

(1977).
[6]H. Weitzel, Solid State Commun. **8**, 2071 (1970).
[7]C. Wilkinson and M. J. Sprague, Z. Kristallogr. **145**, 96 (1977).
[8]H. Weitzel, N. Jahrb. Miner. Abh. **113**, 13 (1970).
[9]H. Weitzel, Z. Kristallogr. **131**, 289 (1970).
[10]C. P. Landee and E. F. Westrum, in *Magnetism and Magnetic Materials,* 1975 Proceedings of the 21st Annual Conference on Magnetism and Magnetic Materials, edited by D. C. Graham and J. J. Rhyne, AIP Conf. Proc. No. 29 (AIP, New York, 1976), pp. 445–446; J. Chem. Thermodyn. **8**, 663 (1976).
[11]P. Bak and J. V. Boehm, Phys. Rev. B **21**, 5297 (1980).
[12]M. E. Fisher and W. Selke, Phys. Rev. Lett. **44**, 1502 (1980).
[13]J. Villain and M. Gordon, J. Phys. C **13**, 3117 (1980).
[14]*The Yellow Book, Guide to Neutron Research Facilities at the ILL,* edited by H. Blank and B. Maier (Institut Max von Laue–Paul Langevin, Grenoble, 1988).
[15]J. Rodriguez-Carvajal, in *Abstracts of the Satellite Meeting of the XV. Congress of the International Union of Crystallography, Toulouse, 1990* (Université Paul Sabatier, Toulouse, 1990), p. 127
[16]O. Elsenhans, J. Appl. Crystallogr. **23**, 73 (1990).
[17]E. F. Bertaut, Acta Crystallogr. A **24**, 217 (1968).
[18]W. Prandl, Z. Kristallogr. **144**, 198 (1976).
[19]W. Prandl, in *Neutron Diffraction,* edited by H. Dachs (Springer, New York, 1978).
[20]Yu. A. Izyumov, V. E. Naish, and R. P. Ozerov, *Neutron Diffraction of Magnetic Materials* (Consultants Bureau, New York, 1991).
[21]J. Sivardiére, Acta Crystallogr. A **26**, 101 (1970).
[22]H. Langhof, Diplomarbeit, Technische Hochschule, Darmstadt, 1975.
[23]C. Wilkinson, G. Lautenschläger, R. Hock, and H. Weitzel, J. Appl. Crystallogr. **24**, 365 (1991).
[24]E. Legrand, S. Hautecler, W. Wegener, and G. Will, J. Magn. Magn. Mater. **15-18**, 529 (1980).
[25]J. Sólyom, Physica **32**, 1243 (1966).